

UniHPE: Towards Unified Human Pose Estimation via Contrastive Learning

Zhongyu Jiang¹ Wenhao Chai¹ Lei Li² Zhuoran Zhou¹
 Cheng-Yen Yang¹ Jenq-Neng Hwang¹

University of Washington¹ University of Copenhagen²

{zyjiang, wchai, zhouz47, cycyang, hwang}@uw.edu, lilei@di.ku.dk

Abstract

In recent times, there has been a growing interest in developing effective perception techniques for combining information from multiple modalities. This involves aligning features obtained from diverse sources to enable more efficient training with larger datasets and constraints, as well as leveraging the wealth of information contained in each modality. 2D and 3D Human Pose Estimation (HPE) are two critical perceptual tasks in computer vision, which have numerous downstream applications, such as Action Recognition, Human-Computer Interaction, Object tracking, etc. Yet, there are limited instances where the correlation between Image and 2D/3D human pose has been clearly researched using a contrastive paradigm. In this paper, we propose **UniHPE**, a unified Human Pose Estimation pipeline, which aligns features from all three modalities, i.e., 2D human pose estimation, lifting-based and image-based 3D human pose estimation, in the same pipeline. To align more than two modalities at the same time, we propose a novel singular value based contrastive learning loss, which better aligns different modalities and further boosts the performance. In our evaluation, UniHPE achieves remarkable performance metrics: MPJPE 50.5mm on the Human3.6M dataset and PAMPJPE 51.6mm on the 3DPW dataset. Our proposed method holds immense potential to advance the field of computer vision and contribute to various applications.

1. Introduction

Estimating 2D and 3D human poses (i.e., human keypoints) from only RGB images is one of the foundational tasks in the computer vision field, which can be further used for several downstream tasks like multiple object tracking [1, 42], action recognition [7, 41], human-computer interaction [16, 54], human body reconstruction [26, 55], sports application [18, 64], etc. Previous works follow the paradigms which estimate 3D human poses from 2D hu-

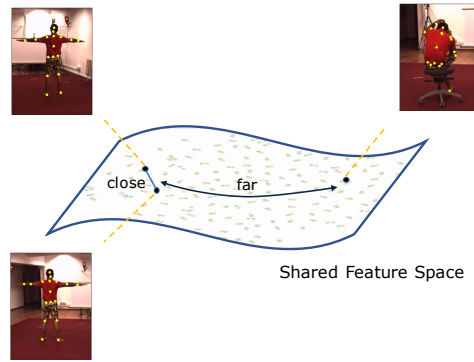


Figure 1. RGB image, 2D and 3D human pose embeddings extracted by corresponding encoders in the shared feature space. We show that after conducting contrastive learning during the pre-training stage, the embeddings of different modalities from the same sample are close to each other and away from other negative samples.

man poses (so-called lifting) [12, 33, 39, 63, 65] or directly regress 3D human poses from RGB images (image-based) [8, 24, 47, 48, 59, 60]. Lifting networks learn the mapping between 2D and 3D human poses, and the image-based methods take advantage of the rich image information to get accurate pose estimation results. Yet, the lifting method remains a two-stage paradigm heavily reliant on the efficacy of 2D human pose detectors in the first phase. On the other hand, the absence of large-scale and diverse image-3D pose pairs data for training hurts the generalization of image-based methods. This brings up the question: *Can we establish a unified human pose estimation paradigm by taking advantage of both lifting and image-based methods?*

From the perspective of representation learning, previous methods have been dedicated to mapping the representation of RGB images or 2D poses into the corresponding 3D pose space. In this paper, we propose UniHPE, a Unified Human Pose Estimation framework, which aims to align RGB im-

age, 2D and 3D human pose in the shared feature space in the pre-training stage, to further benefit pose estimation tasks. UniHPE can conduct 2D human pose estimation, lifting-based 3D human pose estimation, and image-based human pose estimation in a single model.

Learning joint embeddings across more than two modalities is a challenge. Inspired by Contrastive Language-Image Pre-Training (CLIP) [40], which proposes to learn transferable visual features with natural language supervisions trained on web-scale image-text pairs data, we claim that RGB image, 2D and 3D human pose representation alignment can also benefit from contrastive learning on large-scale and diverse datasets (*e.g.*, Human3.6M [17], MPI-INF-3DHP [34], *etc.*).

Our proposed framework follows the encoder-decoder architecture, consisting of image, 2D and 3D human pose encoders, and 2D and 3D human pose decoders. The embedding features of these three modalities are shared in the bottleneck. To be specific, we first encode the images by HRNet [52], 2D and 3D human poses by Transformer [50] respectively to get the corresponding embeddings. During the pre-training stage, we conduct contrastive learning to force the embeddings of different modalities from the same training sample to be close in the shared feature space. However, aligning more than two modalities is challenging, and therefore, we propose a singular value based contrastive learning loss to align three modalities at the same time. After that, during the training stage, we jointly train encoders and decoders with contrastive learning and multi-task learning simultaneously. During inference, since the embeddings are aligned in the same feature space, UniHPE supports 2D human pose estimation and lifting-based and image-based 3D human pose estimation in the same pipeline.

Our contributions can be summarised as follows:

- UniHPE can conduct both 2D and 3D HPE tasks in a single model and take advantage of both lifting and image-based 3D HPE methods.
- We show that HPE tasks can benefit from feature alignment pre-training via contrastive learning.
- We propose singular value based InfoNCE loss for contrastive learning to align more than two modalities at the same time.
- UniHPE achieves MPJPE 50.5 mm on the Human3.6M dataset and PAMPJPE 51.6 mm on the 3DPW dataset.

2. Related Works

Traditionally, the estimation of 3D human poses [53] has been achieved by mainly two approaches: 2D-3D lifting and image-based method.

2.1. Lifting Method for 3D HPE

2D-3D lifting [4, 12, 19, 33, 39, 63, 66] methods aim to infer 3D human pose under the assistance of 2D joint detector. Thus, the relations between 2D and 3D human poses have captivated the attention of numerous researchers in computer vision and human motion analysis. Though the internal correspondence is tight, it is rather challenging to connect their representations in the same embedding space as they contain various spatial information, and ambiguities in depth may also cause severe one-to-many 2D-3D mappings.

2.2. Image-based Method for 3D HPE

The other approach for estimating 3D human poses is building an end-to-end network designed to predict the 3D joint coordinates of the poses or SMPL[30] parameters directly from RGB images. Those methods can be categorized into two main classes: heatmap-based [32, 37] and regression-based [22–24, 26, 28, 38, 59] methods. Following the architecture of 2D human pose estimation, heatmap-based methods generate a 3D likelihood heatmap for each individual joint, and the joint’s position is ascertained by identifying the peak within the heatmap. On the other hand, the regression-based methods detect the root location and regress the relative locations of other joints in two branches. In contrast, the SMPL regression methods focus on regressing SMPL parameters from image or video input. Kolotouros *et al.* [24] propose SPIN, which takes advantage of an optimization-based 3D pose estimation method, *i.e.*, SMPLify [3], to achieve semi-supervised learning on 2D pose only datasets. VIBE [22] utilizes temporal information and a discriminator pretrained on a large 3D pose dataset to enhance the performance.

2.3. Multi-Modal Learning and Feature Alignment

How to align data from multiple modalities is a challenging and important task. CLIP [40] is trained on web-scale text-image pairs under a contrastive learning paradigm. Inspired by the outstanding capability of learning representations for both vision and language of CLIP, various models have adopted the contrastive method to pursue zero-shot performance in other areas, such as [11, 14, 29, 31], by pre-training the model which maximizes cross-modal similarity scores. In this process, CLIP-based models would automatically learn implicit multi-modal alignments, which intensively reduces the difficulty of manually building feature correspondence. However, the majority of prior research has predominantly concentrated on visual-language or other visual-related cross-modal capacity, primarily due to the substantial availability of image-text paired datasets. Nonetheless, few works focus on the area of human pose. MPM [62] aims to learn shared 2D-3D human pose features

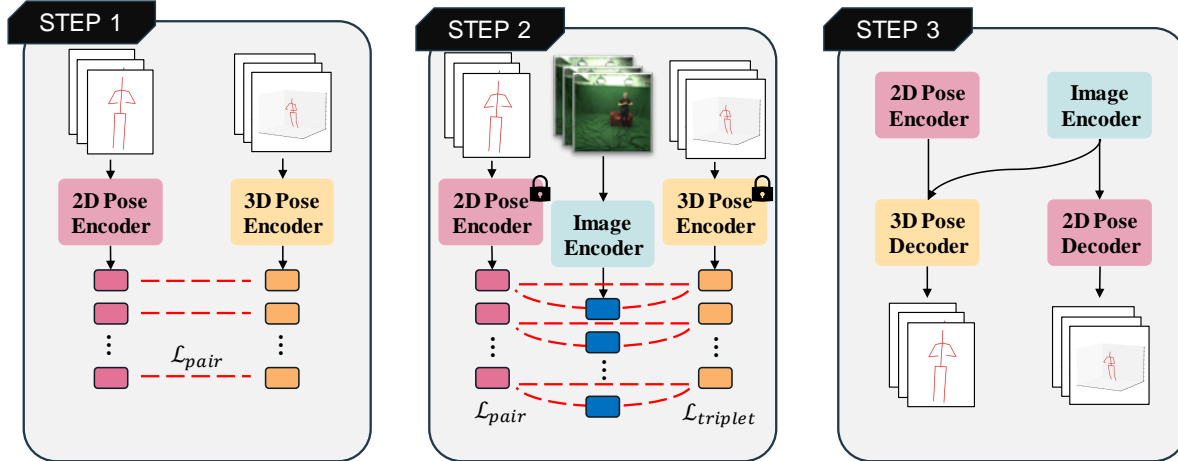


Figure 2. The training scheme of **UniHPE**. Steps 1 and 2 are pre-training stages, and Step 3 is for multi-task learning. During Step 1, we train the 2D and 3D pose embedding alignment first with \mathcal{L}_{pair} , and in Step 2, the image encoder is aligned with frozen 2D and 3D pose encoders via \mathcal{L}_{pair} and $\mathcal{L}_{triplet}$. In Step 3, encoders and decoders are trained jointly via both contrastive learning and multi-task learning.

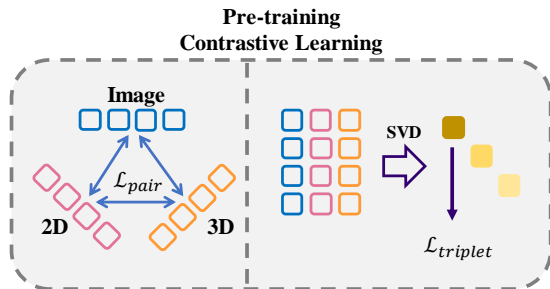


Figure 3. \mathcal{L}_{pair} is applied three times for contrastive learning and the singular value based $\mathcal{L}_{triplet}$ focuses on aligning three modalities at the same time.

by the masked modeling paradigm. Yet, there are limited instances where the correlation between 2D/3D human pose has been clearly researched using a contrastive paradigm similar to our method. Furthermore, we further align image features with 2D and 3D human pose features and construct our unified human pose estimation pipeline.

3. Methodology

We build a unified human pose estimation pipeline. During training, for any triplet of the cropped human image, $I \in \mathbb{N}^{H \times W \times 3}$, 2D and 3D human pose, $P_{2D/3D} \in \mathbb{R}^{J \times 2/3}$, UniHPE aligns the embeddings from all three modalities and utilizes 2D and 3D pose decoders for downstream tasks.

3.1. Framework Architecture

Image encoder. We simply use HRNet [52] to extract the embeddings from RGB images, which is a convolution-based backbone for various visual recognition tasks. We

concatenate and flatten the average pooled feature maps from the last stage and pass it through a linear projection layer to get a 1-D embedding vector as our image embedding.

2D/3D pose encoder. We adopt Transformer-based [50] encoders to extract the embeddings from 2D and 3D human poses. We conduct bounding box normalized keypoint-wise patch embedding and retain the spatial information of each keypoint via adding learnable spatial position embedding. Then, the pose tokens prepended with a $[CLS]$ token and a bounding box token are fed into standard transformer encoder layers, including multi-head self-attention, feed-forward layers, and normalization layers. After that, we use the $[CLS]$ tokens as the 2D and 3D human pose embedding, respectively, which aggregates the information of the other tokens and can be regarded as general prior.

2D and 3D pose decoder. We build diffusion-based modules, $\mathcal{D}_{2D/3D}$, with two residual blocks to decode the embeddings and get 2D and 3D human poses. We treat the decoders following the Score Matching paradigm [44] instead of DDPM[15] or DDIM[43]. To be specific, the encoded embeddings are added with time embedding as well as a modality token, which indicates the source of the embedding (e.g. from an image, 2D or 3D pose) in the diffusion network as condition embeddings and are used to generate the final 2D and 3D poses.

We also try different architectures of encoders and decoders in the ablation study Section 4.4.

Algorithm 1 Random Sampling in \mathcal{L}_{svd}

Require: Image embeddings, x_{img} , 2D pose embeddings, x_{2D} , 3D pose embeddings, x_{3D}
Batch size, B

```
index_list ← zeros( $B, B, 3$ )
for  $i \leftarrow 0, B$  do
  index_list[:,  $i, 0$ ] ← arange( $B$ )
  index_list[:,  $0, i$ ] ← arange( $B$ )
end for
for  $i \leftarrow 1, B$  do
  for  $j \leftarrow 1, 3$  do
    index_list[:,  $i, j$ ] ← shuffle(arange( $B$ ))
  end for
end for
```

Algorithm 1. The **pseudo-code** of triplet random sampling and the implementation of $\mathcal{L}_{triplet}$. To simplify the computation, for each mini batch, we randomly sample $B - 1$ negative triplets and one positive triplet. In

3.2. Pre-training via Contrastive Learning

During the pre-training stage, we aim to align the embeddings from images, 2D and 3D human poses via contrastive learning. Given a batch of data, we have the RGB images, $I \in \mathbb{N}^{B \times H \times W \times 3}$, 2D poses, $P_{2D} \in \mathbb{R}^{B \times J \times 2}$, and 3D poses, $P_{3D} \in \mathbb{R}^{B \times J \times 3}$, where B, H, W, J are batch size, image height and width, and number of joints. We aim to train the image, 2D, and 3D pose encoders E_{img}, E_{2D}, E_{3D} by maximizing the similarity between image embeddings $x_{img} \in \mathbb{R}^{B \times D}$, 2D pose embeddings $x_{2D} \in \mathbb{R}^{B \times D}$, and 3D pose embeddings $x_{3D} \in \mathbb{R}^{B \times D}$, where D is the dimension of the embeddings, which is the same over three modalities. The most intuitive approach to aligning three modalities is to apply three pair-wise contrastive loss functions. For embeddings, x_S, x_T , from any pair of modalities, the contrastive learning loss is

$$\mathcal{L}_{pair} = -\log \frac{\exp(x_S \cdot x_T^+ / \tau)}{\sum_{i=1}^B \exp(x_S \cdot x_{T,i} / \tau)}, \quad (1)$$

where τ is the learnable temperature initialized by τ_0 .

However, we found that simply applying three pairwise InfoNCE loss cannot obtain expected embedding similarity across three modalities, as shown in the ablation studies Section 4.4. Therefore, we propose a singular value-based InfoNCE loss (Triplet-InfoNCE) to address this issue.

We stack the embeddings from three modalities to build a normalized embedding matrix formulated by

$$\mathcal{M}_x = [x_{img} \quad x_{2D} \quad x_{3D}]^T \in \mathbb{R}^{3 \times D}. \quad (2)$$

If we apply singular value decomposition (SVD) to this matrix, $M_x = U \Sigma V^*$, the largest singular value, $\sigma_1 = \Sigma_{11}$,

Algorithm 2 Implementation of \mathcal{L}_{svd}

Require: Normalized image embeddings, x_{img} 2D pose embeddings, x_{2D} , 3D pose embeddings, x_{3D} ,
Batch size, B , Temperature, τ

```
 $\mathcal{M}_x \leftarrow \text{stack}((x_{img}, x_{2D}, x_{3D}), \text{dim} = 1)$ 
index_list ← RandSample( $x_{img}, x_{2D}, x_{3D}$ )
#  $\mathcal{M}_x \in \mathbb{R}^{B \times B \times 3 \times D}$ 
 $\mathcal{M}_x \leftarrow \mathcal{M}_x[\text{index\_list}]$ 
#  $\mathcal{M}_x \in \mathbb{R}^{B \times B \times 3 \times 3}$ 
 $\mathcal{M}_x \leftarrow \mathcal{M}_x \mathcal{M}_x^T$ 
logits ← eigenval( $\mathcal{M}_x$ )[:, :, 0]
logits ← logits /  $\tau$ 
label ← zeros( $B$ )
 $\mathcal{L}_{triplet} = \text{CrossEntropy}(\text{logits}, \text{label})$ 
```

is related to the linear correlation of row vectors. Meanwhile, since the embeddings are normalized, the largest singular value should be in $[-\sqrt{3}, \sqrt{3}]$. Therefore, we can use InfoNCE loss to align any triplet of embeddings by maximizing the σ_1 . However, computing the singular value of a matrix with $3 \times D$, where $3 \ll D$, is time-consuming. In our implementation, the largest eigenvalue λ_1 of the matrix $\mathcal{M}_x \mathcal{M}_x^T \in \mathbb{R}^{3 \times 3}$ is our optimization target, since $\lambda_1 = \sigma_1^2$. Therefore, by maximizing the λ_1 for positive triplets, which contain three embeddings from the same frame, and minimizing the λ_1 for negative triplets, which contain at least one embedding from a different frame, we are able to align embeddings from three modalities jointly.

However, in one mini batch, the number of negative triplets for any positive triplet is $3B^2 - 3B + 1$, and if we use all the negative samples as our denominator in InfoNCE loss, the time consumption is unacceptable. As shown in the Alg 1, we apply a random sample algorithm to select only $B - 1$ negative triplets for each positive triplet. In this case, the singular value based InfoNCE loss can be formed as,

$$\mathcal{L}_{triplet} = -\log \frac{\exp(\lambda_1^+ / \tau)}{\sum_{i=1}^B \exp(\lambda_{1i} / \tau)}. \quad (3)$$

Overall, our contrastive learning loss is

$$\mathcal{L}_{cl} = \mathcal{L}_{pair} + \alpha \mathcal{L}_{triplet}. \quad (4)$$

where α is the weighted factor.

3.3. Training via Multi-Task Learning

After the pre-training stage, all encoders and decoders are trained jointly. While encoders are trained with \mathcal{L}_{cl} , the

Method		3DPW	Human3.6M	
		PA-MPJPE (\downarrow)	MPJPE (\downarrow)	PA-MPJPE (\downarrow)
Temporal	VideoPose3D (f=243) [39]	68.0	46.8	36.5
	AdaptPose [10]	46.5	-	-
	Li <i>et al.</i> [27]	-	43.7	35.2
	MixSTE [61]	-	40.9	32.6
	MPM [62]	-	42.6	34.7
Frame-based	SimpleBaseline [33]	89.4	62.9	47.7
	SemGCN [63]	102.0	61.2	47.7
	VideoPose3D (f=1) [39]	94.6	55.2	42.3
	PoseAug [12]	58.5	52.9	-
	PoseDA [4]	55.3	-	-
	UniHPE (ours)	51.6	<u>53.6</u>	40.9

Table 1. **Lifting-based 3D HPE** performance on the 3DPW and Human3.6M datasets under MPJPE and PA-MPJPE. The ground truth 2D keypoints are used on 3DPW dataset, while the detected 2D keypoints from CPN are used on Human3.6M dataset.

task losses, $\mathcal{L}_{2D/3D}$, depend on the architectures of decoders. For diffusion-based decoders, we adopt the loss from the Score Matching Network [45], and for MLP-based decoders, we utilize simple mean square error losses.

Therefore, the overall loss is

$$\mathcal{L} = \mathcal{L}_{cl} + \mathcal{L}_{2D} + \mathcal{L}_{3D}. \quad (5)$$

During inference, since the embeddings are aligned in the same feature space, UniHPE can support 2D human pose estimation and lifting-based and image-based 3D human pose estimation in the same pipeline. The 2D human pose can be estimated by sending the image embedding to the 2D decoder and the 3D human pose can be predicted by sending 2D or image embedding to the 3D decoder.

4. Experiments

4.1. Datasets and Performance Metrics

We use several widely used 3D human pose datasets to train and evaluate our framework, including Human3.6M [17], MPI-INF-3DHP [34], and 3DPW [51]. We train UniHPE on Human3.6M and 3DHP datasets and evaluate it on Human3.6M and 3DPW datasets.

Human3.6M Human3.6M [17] dataset, which contains 3.6 million frames of corresponding 2D and 3D human poses, including 5 female and 6 male subjects under 17 different scenarios, is a video dataset captured using a Mo-Cap system. Following the previous works, we choose 5 subjects (S1, S5, S6, S7, S8) for training, and the other 2 subjects (S9 and S11) for evaluation. We report the Mean Per Joint Position Error (MPJPE) as the performance metric of Protocol #1 as well as Procrustes analysis MPJPE (PA-MPJPE) as the metric of Protocol #2 for both the lifting path and image-bath path in our proposed framework.

MPI-INF-3DHP Compared to Human3.6M, MPI-INF-3DHP [34] is a more challenging 3D human pose dataset captured indoors and outdoors. MPI-INF-3DHP contains 1.3 million frames, consisting of 4 males and 4 females with 8 types of action captured by 14 cameras covering a greater diversity of poses. We use MPI-INF-3DHP in training to enrich the training samples and enhance the performance of our image branch.

3DPW 3DPW [51] is the first dataset that includes video footage taken from a moving phone camera. It includes 60 video sequences as the training dataset with 22k images, while the testing dataset includes 35k images. Compared to Human 3.6M or MPI-INF-3DHP, 3DPW is a more challenging in-the-wild dataset, with uncontrolled motion and scene. Similar to most other works, we only evaluate our model under PA-MPJPE metrics, without considering MPJPE, due to the fact that the scale of the human body, camera intrinsic, and distance of 3DPW are not compatible with the training data.

4.2. Implementation Details

Training settings. We implement our proposed framework using PyTorch [36] on a single NVIDIA A100 80G GPU. The pre-training includes two stages: (1) 2D-3D alignment; (2) Image-2D-3D joint alignment. In the first stage of pre-training, the batch size is 2048, $\tau_0 = 1/14$, and $\tau \in [1/100, 10^4]$, while in the second stage, the batch size is 180, $\tau_0 = 1/5$, and $\tau \in [1/10, 10^4]$. During the multi-task training stage, encoders and decoders are trained together with the batch size being 180, $\tau_0 = 1/5$, and $\tau \in [1/5, 10^4]$. For the weight of triplet contrastive loss, $\mathcal{L}_{triplet}$, $\alpha = 1$. The input image size of the image encoder is 192×256 . During both of the two stages, we adopt Adam optimizer with a learning rate of 1×10^{-4} . We train UniHPE on Human3.6M [17] and MPI-INF-3DHP [34] datasets and

Method	3DPW	Human3.6M		
	PA-MPJPE (\downarrow)	MPJPE (\downarrow)	PA-MPJPE (\downarrow)	
Temporal	Kanazawa <i>et al.</i> [21]	72.6	-	56.9
	Doersch <i>et al.</i> [6]	74.7	-	-
	Arnab <i>et al.</i> [2]	72.2	77.8	54.3
	DSD [46]	69.5	59.1	42.4
	VIBE [22]	56.5	65.9	41.5
	Pavliakos <i>et al.</i> [38]	-	-	75.9
Frame-based	HMR [20]	76.7	88.0	56.8
	NBF [35]	-	-	59.9
	GraphCMR [25]	70.2	-	50.1
	HoloPose [13]	-	60.3	46.5
	DenseRaC [56]	-	76.8	48.0
	SPIN [24]	59.2	62.5	41.1
	DecoMR [58]	61.7	-	39.3
	HKMR [9]	-	59.6	43.2
	PyMAF [59]	58.9	57.7	40.5
	PARE [23]	50.9	76.8	50.6
	PyMAF-X [60]	47.1	54.2	37.2
	CLIFF [28]	43.0	47.1	32.7
	UniHPE-w32 (ours)	67.1	55.2	40.0
	UniHPE-w48 (ours)	65.7	<u>50.5</u>	<u>36.2</u>

Table 2. **Image-based 3D HPE** performance on the 3DPW and Human3.6M datasets under MPJPE and PA-MPJPE.

apply ablation study about the performance difference of using different training datasets.

4.3. Comparison with State-of-the-Art Methods

Lifting-based 3D Human Pose Estimation We evaluate the performance of lifting-based 3D HPE tasks on Human3.6M and 3DPW datasets. As shown in Table 1, UniHPE archives 51.6 mm in terms of PA-MPJPE on 3DPW dataset and 53.6 mm in terms of MPJPE on Human3.6M dataset, which is the state-of-the-art performance. Since UniHPE is not trained on 3DPW, it is a fair comparison with those cross-domain evaluation methods.

Image-based 3D Human Pose Estimation As for image-based 3D HPE, we also evaluate the performance on Human3.6M and 3DPW datasets. As shown in Table 2, UniHPE archives 50.5 mm and 36.2 mm in terms of MPJPE and PA-MPJPE on Human3.6M dataset, as well as 65.7 mm of PA-MPJPE on 3DPW dataset. Note that we are the only keypoint-based method in the Table 2, and all the others are SMPL-based. UniHPE archives competitive results regarding the number of model parameters and training data with SOTA methods, showing the effectiveness of our method.

2D Human Pose Estimation Since our pipeline also supports 2D pose estimation, we compare the 2D pose estimation performance of UniHPE with the SOTA method on the Human3.6M dataset. The evaluation metrics are Percentage of Correct Keypoints (PCK) with a threshold as 0.05 and End Point Errors (EPE). As shown in Table 3,

Model	PCK _{0.05} (\uparrow)	EPE (\downarrow)
HRNet-w32	91.1	9.43
HRNet-w48	93.2	7.36
UniHPE-w32	93.5	7.18

Table 3. 2D Pose Estimation on Human3.6M dataset. UniHPE with HRNet-w32 as the image encoder outperforms the original HRNet-w32 and even HRNet-w48.

2D Encoder	3D Decoder	MPJPE (\downarrow)	PA-MPJPE (\downarrow)
MLP	MLP	60.5	44.5
transformer	MLP	64.8	48.1
MLP	diffusion	71.4	45.6
transformer	diffusion	39.3	29.9

Table 4. **Ablation study** on architecture selection in lifting-based 3D HPE task. Evaluated on Human3.6M dataset with ground truth 2D keypoints.

image Encoder	MPJPE (\downarrow)	PA-MPJPE (\downarrow)
ViT-S	151.6	93.8
ViT-B	149.9	93.4
HRNet-w32	55.2	40.0
HRNet-w48	50.5	36.2

Table 5. **Ablation study** on image encoder architecture selection in image-based 3D HPE task. Evaluated on Human3.6M dataset.

the UniHPE with HRNet-w32 as backbone can even outperform the original HRNet-w48 with PCK_{0.05} as 93.5 and EPE as 7.18.

4.4. Ablation Study

In this section, we conduct extensive ablation studies to investigate the importance of each module in the UniHPE, especially how the singular value based loss, \mathcal{L}_{triple} , helps the training.

Encoder and decoder architecture. Since UniHPE is flexible with any encoder or decoder architecture, we conduct experiments on several strong backbones with different architectures, including MLP, CNN, transformer, and diffusion. We first select HRNet-w32 as the image encoder during alignment training and evaluate the performance of the lifting branch under different combinations of 2D pose encoder and 3D pose decoder architecture in the 3D HPE task on the Human3.6M dataset. As shown in Table 4, transformer-based 2D pose encoder and diffusion-based 3D pose encoder achieve the best performance. Then, we keep this selection and further conduct ablation studies in the image encoder part. As shown in Table 5, HRNet-w48 outperforms then other encoders in the image-based 3D HPE task on the Human3.6M dataset. We utilize the coco pre-

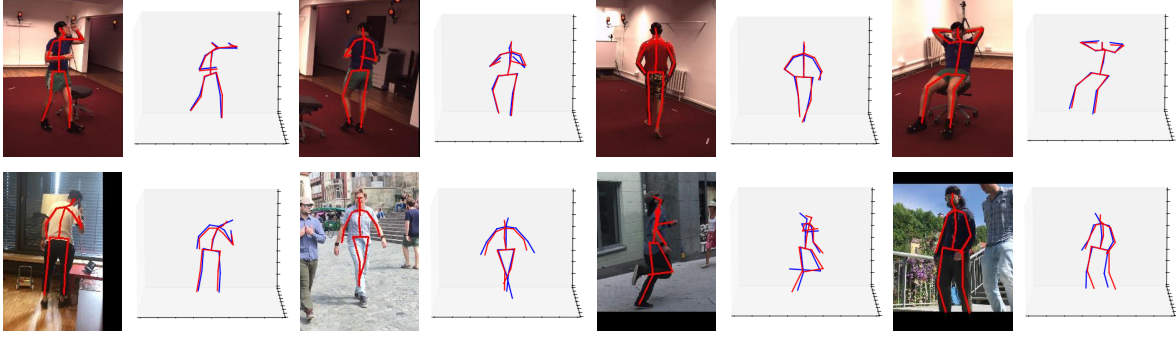


Figure 4. Qualitative results on Human3.6M (row 1) and 3DPW (row 2) datasets. Red poses are ground truth, and the blue ones are estimated from the image branch.

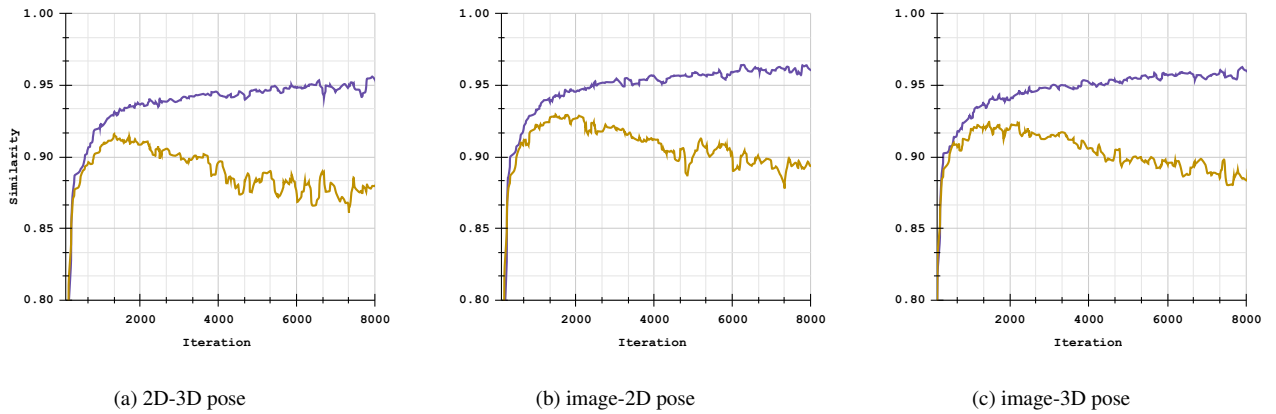


Figure 5. **Cosine similarities** between different modalities. The yellow line is the one only trained with three pair-wise losses, \mathcal{L}_{pair} , and the purple line is the training curve with additional singular value-based InfoNCE loss, $\mathcal{L}_{triplet}$. Our proposed singular value-based InfoNCE loss helps align the feature space.

trained HRNet and ViTPose[57] as the initial weights for a fair comparison.

End-to-End training without alignment. We claim that feature alignment, pre-training via contrastive learning, between different modalities is the key to success. Therefore, we conduct the ablation studies on skipping the alignment training stages. As shown in Table 6, alignment improves the image-based 3D HPE performance significantly on the Human3.6M dataset. As shown in table 6, without contrastive learning, the performance gap between lifting and image branches shows that the features are not correctly aligned. Furthermore, the combination of $\mathcal{L}_{triplet}$ and \mathcal{L}_{pair} provides the best performance on both lifting and image branches, which matches with the comparative results shown in Fig 5.

Ablation on modality token. In UniHPE, we design a modality token when using the 3D pose decoder to estimate 3D human poses. The modality token indicates which

modality the features came from (*e.g.* image or 2D pose). As shown in Table 6, consistent improvement is observed in using the modality token among lifting-based and image-based 3D HPE tasks on the Human3.6M dataset.

Training objective in pre-training. We conduct training objectives in the alignment training stage. As shown in Figure 5, compared to simply applying three pairwise InfoNCE loss, \mathcal{L}_{pair} , the proposed singular value-based InfoNCE loss, $\mathcal{L}_{triplet}$, significantly better aligns the feature from different modality. With the help of $\mathcal{L}_{triplet}$, the embedding cosine similarity between different modalities does not decrease after around 1500 iterations and keeps increasing to around 0.95 in 8000 iterations.

Training with additional data. As shown in Table 6, by training the UniHPE on an additional dataset, like 3DHP, the performance of the lifting-based 3D pose estimation drops, but the image-based branch improves. It is noted that the distribution of 2D and 3D pose pairs on 3DHP differs

\mathcal{L}_{pair}	$\mathcal{L}_{triplet}$	\mathcal{M} Token	+3DHP	GT 2D		Image	
				MPJPE (\downarrow)	PA-MPJPE (\downarrow)	MPJPE (\downarrow)	PA-MPJPE (\downarrow)
				41.3	31.6	91.8	68.7
✓				60.0 (+18.7)	47.5 (+15.9)	65.5 (-26.3)	51.8 (-16.9)
✓	✓			40.9 (-0.4)	31.7 (+0.1)	58.7 (-33.1)	44.4 (-24.3)
✓	✓	✓		39.3 (-2.0)	29.9 (-1.7)	57.5 (-34.3)	42.9 (-25.8)
✓	✓	✓	✓	44.2 (+2.9)	33.6 (+2.0)	55.1 (-36.7)	40.0 (-28.7)

Table 6. **Ablation study** on UniHPE. Evaluated on Human3.6M dataset. \mathcal{L}_{pair} and $\mathcal{L}_{triplet}$ denotes applying those losses on the pre-training stage. \mathcal{M} token means decoders utilize the modality token. We evaluate the performance with additional data from MPI-INF-3DHP dataset as well.

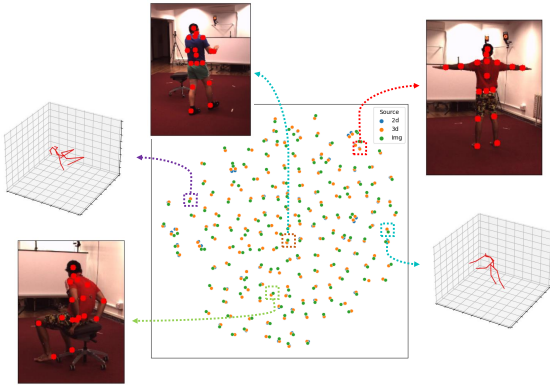


Figure 6. The visualization of the shared feature space from UniHPE using t-SNE. The features of different modalities are aligned with each other and uniformly distributed in the shared feature space.

from Human3.6M, which increases the robustness of the lifting-based branch but decreases the performance on Human3.6M. However, the training with additional data boosts the image-based branch by improving the image data diversity.

Visualization of Shared Feature Space. As shown in Fig 6, embeddings of different modalities are aligned with each other and uniformly distributed in the shared feature space. The visualization is based on t-SNE[49].

Failure cases. As shown in Figure 7, the image branch of UniHPE fails in the case of large occlusion or low-quality RGB input scenarios. UniHPE is trained on Human3.6M and MPI-INF-3DHP with only one target per frame and a limited amount of occlusion.

5. Limitation and Future Work

Moreover, our proposed UniHPE relies on the availability of large-scale and diverse datasets for pre-training using



Figure 7. Failure cases of UniHPE. When there is heavy occlusion, our model may estimate the incorrect pose or the pose of a wrong target.

contrastive learning. While the approach aligns RGB image, 2D, and 3D human pose representations in a shared feature space, its performance is likely contingent on the diversity and amount of data it is trained on. This could bring challenges in environments where such rich datasets are not available, potentially limiting the model’s ability to generalize to new or rare poses. For our future work, adopting SMPL model may help the pipeline better utilize semi-supervised learning by taking advantage of 2D human pose estimation datasets. Meanwhile, the aligned embeddings and pre-trained model from UniHPE may benefit more downstream tasks, like human re-identification, action recognition, *etc.*

6. Conclusion

In conclusion, the UniHPE framework represents a significant step forward in unified human pose estimation by integrating the strengths of lifting and image-based methods within a single model. It leverages contrastive learning to align embeddings across modalities in a shared feature space, enhancing the model’s accuracy in pose estimation tasks. Despite its potential limitations in data requirements and computational intensity, UniHPE sets a promising direction for future research, particularly in improving generalization capabilities and a unified end-to-end pipeline. The framework’s achievements on benchmark datasets like Human3.6M and 3DPW underscore its potential, paving the way for advancements in applications across multiple domains such as motion analysis, augmented reality, and human-computer interaction.

References

- [1] Mykhaylo Andriluka, Umar Iqbal, Eldar Insafutdinov, Leonid Pishchulin, Anton Milan, Juergen Gall, and Bernt Schiele. Posetrack: A benchmark for human pose estimation and tracking. In *Proceedings of the IEEE conference on computer vision and pattern recognition*, pages 5167–5176, 2018. [1](#)
- [2] Anurag Arnab, Carl Doersch, and Andrew Zisserman. Exploiting temporal context for 3d human pose estimation in the wild. In *Proceedings of the IEEE/CVF Conference on Computer Vision and Pattern Recognition*, pages 3395–3404, 2019. [6](#)
- [3] Federica Bogo, Angjoo Kanazawa, Christoph Lassner, Peter Gehler, Javier Romero, and Michael J Black. Keep it smpl: Automatic estimation of 3d human pose and shape from a single image. In *Computer Vision—ECCV 2016: 14th European Conference, Amsterdam, The Netherlands, October 11–14, 2016, Proceedings, Part V 14*, pages 561–578. Springer, 2016. [2](#)
- [4] Wenhao Chai, Zhongyu Jiang, Jenq-Neng Hwang, and Gaoang Wang. Global adaptation meets local generalization: Unsupervised domain adaptation for 3d human pose estimation. *arXiv preprint arXiv:2303.16456*, 2023. [2](#), [5](#)
- [5] Hai Ci, Mingdong Wu, Wentao Zhu, Xiaoxuan Ma, Hao Dong, Fangwei Zhong, and Yizhou Wang. Gfpose: Learning 3d human pose prior with gradient fields. In *Proceedings of the IEEE/CVF Conference on Computer Vision and Pattern Recognition*, pages 4800–4810, 2023. [2](#)
- [6] Carl Doersch and Andrew Zisserman. Sim2real transfer learning for 3d human pose estimation: motion to the rescue. *Advances in Neural Information Processing Systems*, 32, 2019. [6](#)
- [7] Haodong Duan, Jiaqi Wang, Kai Chen, and Dahua Lin. Pyskl: Towards good practices for skeleton action recognition. In *Proceedings of the 30th ACM International Conference on Multimedia*, pages 7351–7354, 2022. [1](#)
- [8] Georgios Georgakis, Ren Li, Srikrishna Karanam, Terrence Chen, Jana Košecká, and Ziyang Wu. Hierarchical kinematic human mesh recovery. In *Computer Vision—ECCV 2020: 16th European Conference, Glasgow, UK, August 23–28, 2020, Proceedings, Part XVII 16*, pages 768–784. Springer, 2020. [1](#)
- [9] Georgios Georgakis, Ren Li, Srikrishna Karanam, Terrence Chen, Jana Košecká, and Ziyang Wu. Hierarchical kinematic human mesh recovery. In *Computer Vision—ECCV 2020: 16th European Conference, Glasgow, UK, August 23–28, 2020, Proceedings, Part XVII 16*, pages 768–784. Springer, 2020. [6](#)
- [10] Mohsen Gholami, Bastian Wandt, Helge Rhodin, Rabab Ward, and Z Jane Wang. Adaptpose: Cross-dataset adaptation for 3d human pose estimation by learnable motion generation. In *Proceedings of the IEEE/CVF Conference on Computer Vision and Pattern Recognition*, pages 13075–13085, 2022. [5](#)
- [11] Rohit Girdhar, Alaeldin El-Nouby, Zhuang Liu, Mannat Singh, Kalyan Vasudev Alwala, Armand Joulin, and Ishan Misra. Imagebind: One embedding space to bind them all. In *Proceedings of the IEEE/CVF Conference on Computer Vision and Pattern Recognition*, pages 15180–15190, 2023. [2](#)
- [12] Kehong Gong, Jianfeng Zhang, and Jiashi Feng. Poseaug: A differentiable pose augmentation framework for 3d human pose estimation. In *Proceedings of the IEEE/CVF conference on computer vision and pattern recognition*, pages 8575–8584, 2021. [1](#), [2](#), [5](#)
- [13] Riza Alp Guler and Iasonas Kokkinos. Holopose: Holistic 3d human reconstruction in-the-wild. In *Proceedings of the IEEE/CVF Conference on Computer Vision and Pattern Recognition*, pages 10884–10894, 2019. [6](#)
- [14] Andrey Guzhov, Federico Raue, Jörn Hees, and Andreas Dengel. Audioclip: Extending clip to image, text and audio. In *ICASSP 2022-2022 IEEE International Conference on Acoustics, Speech and Signal Processing (ICASSP)*, pages 976–980. IEEE, 2022. [2](#)
- [15] Jonathan Ho, Ajay Jain, and Pieter Abbeel. Denoising diffusion probabilistic models. *Advances in neural information processing systems*, 33:6840–6851, 2020. [3](#)
- [16] Jun Hu, Zhongyu Jiang, Xionghao Ding, Taijiang Mu, and Peter Hall. Vgpn: Voice-guided pointing robot navigation for humans. In *2018 IEEE International Conference on Robotics and Biomimetics (ROBIO)*, pages 1107–1112. IEEE, 2018. [1](#)
- [17] Catalin Ionescu, Dragos Papava, Vlad Olaru, and Cristian Sminchisescu. Human3.6m: Large scale datasets and predictive methods for 3d human sensing in natural environments. *IEEE transactions on pattern analysis and machine intelligence*, 36(7):1325–1339, 2013. [2](#), [5](#)
- [18] Zhongyu Jiang, Haorui Ji, Samuel Menaker, and Jenq-Neng Hwang. Golfpose: Golf swing analyses with a monocular camera based human pose estimation. In *2022 IEEE International Conference on Multimedia and Expo Workshops (ICMEW)*, pages 1–6. IEEE, 2022. [1](#)
- [19] Zhongyu Jiang, Zhuoran Zhou, Lei Li, Wenhao Chai, Cheng-Yen Yang, and Jenq-Neng Hwang. Back to optimization: Diffusion-based zero-shot 3d human pose estimation. *arXiv preprint arXiv:2307.03833*, 2023. [2](#)
- [20] Angjoo Kanazawa, Michael J Black, David W Jacobs, and Jitendra Malik. End-to-end recovery of human shape and pose. In *Proceedings of the IEEE conference on computer vision and pattern recognition*, pages 7122–7131, 2018. [6](#)
- [21] Angjoo Kanazawa, Jason Y Zhang, Panna Felsen, and Jitendra Malik. Learning 3d human dynamics from video. In *Proceedings of the IEEE/CVF conference on computer vision and pattern recognition*, pages 5614–5623, 2019. [6](#)
- [22] Muhammed Kocabas, Nikos Athanasiou, and Michael J Black. Vibe: Video inference for human body pose and shape estimation. In *Proceedings of the IEEE/CVF conference on computer vision and pattern recognition*, pages 5253–5263, 2020. [2](#), [6](#)
- [23] Muhammed Kocabas, Chun-Hao P Huang, Otmar Hilliges, and Michael J Black. Pare: Part attention regressor for 3d human body estimation. In *Proceedings of the IEEE/CVF International Conference on Computer Vision*, pages 11127–11137, 2021. [6](#)
- [24] Nikos Kolotouros, Georgios Pavlakos, Michael J Black, and Kostas Daniilidis. Learning to reconstruct 3d human pose

- and shape via model-fitting in the loop. In *ICCV*, 2019. 1, 2, 6
- [25] Nikos Kolotouros, Georgios Pavlakos, and Kostas Daniilidis. Convolutional mesh regression for single-image human shape reconstruction. In *CVPR*, 2019. 6
- [26] Jiefeng Li, Siyuan Bian, Chao Xu, Zhicun Chen, Lixin Yang, and Cewu Lu. Hybrik-x: Hybrid analytical-neural inverse kinematics for whole-body mesh recovery. *arXiv preprint arXiv:2304.05690*, 2023. 1, 2
- [27] Wenhao Li, Hong Liu, Runwei Ding, Mengyuan Liu, Pichao Wang, and Wenming Yang. Exploiting temporal contexts with strided transformer for 3d human pose estimation. *IEEE Transactions on Multimedia*, 25:1282–1293, 2022. 5
- [28] Zhihao Li, Jianzhuang Liu, Zhensong Zhang, Songcen Xu, and Youliang Yan. Cliff: Carrying location information in full frames into human pose and shape estimation. In *European Conference on Computer Vision*, pages 590–606. Springer, 2022. 2, 6, 1
- [29] Ziyi Lin, Shijie Geng, Renrui Zhang, Peng Gao, Gerard de Melo, Xiaogang Wang, Jifeng Dai, Yu Qiao, and Hongsheng Li. Frozen clip models are efficient video learners. In *European Conference on Computer Vision*, pages 388–404. Springer, 2022. 2
- [30] Matthew Loper, Naureen Mahmood, Javier Romero, Gerard Pons-Moll, and Michael J. Black. SMPL: A skinned multi-person linear model. *ACM Trans. Graphics (Proc. SIGGRAPH Asia)*, 34(6):248:1–248:16, 2015. 2
- [31] Huaishao Luo, Lei Ji, Ming Zhong, Yang Chen, Wen Lei, Nan Duan, and Tianrui Li. Clip4clip: An empirical study of clip for end to end video clip retrieval and captioning. pages 293–304. Elsevier, 2022. 2
- [32] Diogo C Luvizon, David Picard, and Hedi Tabia. 2d/3d pose estimation and action recognition using multitask deep learning. In *Proceedings of the IEEE conference on computer vision and pattern recognition*, pages 5137–5146, 2018. 2
- [33] Julieta Martinez, Rayat Hossain, Javier Romero, and James J Little. A simple yet effective baseline for 3d human pose estimation. In *Proceedings of the IEEE international conference on computer vision*, pages 2640–2649, 2017. 1, 2, 5
- [34] Dushyant Mehta, Helge Rhodin, Dan Casas, Pascal Fua, Oleksandr Sotnychenko, Weipeng Xu, and Christian Theobalt. Monocular 3d human pose estimation in the wild using improved cnn supervision. In *3D Vision (3DV), 2017 Fifth International Conference on*. IEEE, 2017. 2, 5
- [35] Mohamed Omran, Christoph Lassner, Gerard Pons-Moll, Peter V. Gehler, and Bernt Schiele. Neural body fitting: Unifying deep learning and model-based human pose and shape estimation. 2018. 6
- [36] Adam Paszke, Sam Gross, Francisco Massa, Adam Lerer, James Bradbury, Gregory Chanan, Trevor Killeen, Zeming Lin, Natalia Gimelshein, Luca Antiga, et al. Pytorch: An imperative style, high-performance deep learning library. *Advances in neural information processing systems*, 32, 2019. 5
- [37] Georgios Pavlakos, Xiaowei Zhou, Konstantinos G Derpanis, and Kostas Daniilidis. Coarse-to-fine volumetric prediction for single-image 3d human pose. In *Proceedings of the IEEE conference on computer vision and pattern recognition*, pages 7025–7034, 2017. 2
- [38] Georgios Pavlakos, Luyang Zhu, Xiaowei Zhou, and Kostas Daniilidis. Learning to estimate 3d human pose and shape from a single color image. In *Proceedings of the IEEE conference on computer vision and pattern recognition*, pages 459–468, 2018. 2, 6
- [39] Dario Pavlo, Christoph Feichtenhofer, David Grangier, and Michael Auli. 3d human pose estimation in video with temporal convolutions and semi-supervised training. In *Proceedings of the IEEE/CVF conference on computer vision and pattern recognition*, pages 7753–7762, 2019. 1, 2, 5
- [40] Alec Radford, Jong Wook Kim, Chris Hallacy, Aditya Ramesh, Gabriel Goh, Sandhini Agarwal, Girish Sastry, Amanda Askell, Pamela Mishkin, Jack Clark, et al. Learning transferable visual models from natural language supervision. In *International Conference on Machine Learning*, pages 8748–8763. PMLR, 2021. 2
- [41] Amir Shahroudy, Jun Liu, Tian-Tsong Ng, and Gang Wang. Ntu rgb+d: A large scale dataset for 3d human activity analysis. In *Proceedings of the IEEE conference on computer vision and pattern recognition*, pages 1010–1019, 2016. 1
- [42] Michael Snower, Asim Kadav, Farley Lai, and Hans Peter Graf. 15 keypoints is all you need. In *Proceedings of the IEEE/CVF Conference on Computer Vision and Pattern Recognition*, pages 6738–6748, 2020. 1
- [43] Jiaming Song, Chenlin Meng, and Stefano Ermon. Denoising diffusion implicit models. *arXiv preprint arXiv:2010.02502*, 2020. 3
- [44] Yang Song and Stefano Ermon. Generative modeling by estimating gradients of the data distribution. In *Advances in Neural Information Processing Systems*. Curran Associates, Inc., 2019. 3
- [45] Yang Song, Jascha Sohl-Dickstein, Diederik P Kingma, Abhishek Kumar, Stefano Ermon, and Ben Poole. Score-based generative modeling through stochastic differential equations. *arXiv preprint arXiv:2011.13456*, 2020. 5, 2
- [46] Yu Sun, Yun Ye, Wu Liu, Wenpeng Gao, Yili Fu, and Tao Mei. Human mesh recovery from monocular images via a skeleton-disentangled representation. In *Proceedings of the IEEE/CVF international conference on computer vision*, pages 5349–5358, 2019. 6
- [47] Yu Sun, Qian Bao, Wu Liu, Yili Fu, Black Michael J., and Tao Mei. Monocular, One-stage, Regression of Multiple 3D People. In *ICCV*, 2021. 1
- [48] Yu Sun, Wu Liu, Qian Bao, Yili Fu, Tao Mei, and Michael J Black. Putting People in their Place: Monocular Regression of 3D People in Depth. In *CVPR*, 2022. 1
- [49] Laurens Van der Maaten and Geoffrey Hinton. Visualizing data using t-sne. *Journal of machine learning research*, 9 (11), 2008. 8
- [50] Ashish Vaswani, Noam Shazeer, Niki Parmar, Jakob Uszkoreit, Llion Jones, Aidan N Gomez, Łukasz Kaiser, and Illia Polosukhin. Attention is all you need. *Advances in neural information processing systems*, 30, 2017. 2, 3
- [51] Timo Von Marcard, Roberto Henschel, Michael J Black, Bodo Rosenhahn, and Gerard Pons-Moll. Recovering accurate 3d human pose in the wild using imus and a moving

- camera. In *Proceedings of the European conference on computer vision (ECCV)*, pages 601–617, 2018. 5
- [52] Jingdong Wang, Ke Sun, Tianheng Cheng, Borui Jiang, Chaorui Deng, Yang Zhao, Dong Liu, Yadong Mu, Mingkui Tan, Xinggang Wang, et al. Deep high-resolution representation learning for visual recognition. *IEEE transactions on pattern analysis and machine intelligence*, 43(10):3349–3364, 2020. 2, 3
- [53] Jinbao Wang, Shujie Tan, Xiantong Zhen, Shuo Xu, Feng Zheng, Zhenyu He, and Ling Shao. Deep 3d human pose estimation: A review. *Computer Vision and Image Understanding*, 210:103225, 2021. 2
- [54] Kang Wang, Rui Zhao, and Qiang Ji. Human computer interaction with head pose, eye gaze and body gestures. In *2018 13th IEEE International Conference on Automatic Face & Gesture Recognition (FG 2018)*, pages 789–789. IEEE, 2018. 1
- [55] Chung-Yi Weng, Brian Curless, Pratul P Srinivasan, Jonathan T Barron, and Ira Kemelmacher-Shlizerman. Humannerf: Free-viewpoint rendering of moving people from monocular video. In *Proceedings of the IEEE/CVF conference on computer vision and pattern Recognition*, pages 16210–16220, 2022. 1
- [56] Yuanlu Xu, Song-Chun Zhu, and Tony Tung. Denserac: Joint 3d pose and shape estimation by dense render-and-compare. In *Proceedings of the IEEE/CVF International Conference on Computer Vision*, pages 7760–7770, 2019. 6
- [57] Yufei Xu, Jing Zhang, Qiming Zhang, and Dacheng Tao. Vitpose: Simple vision transformer baselines for human pose estimation. *Advances in Neural Information Processing Systems*, 35:38571–38584, 2022. 7
- [58] Wang Zeng, Wanli Ouyang, Ping Luo, Wentao Liu, and Xiaogang Wang. 3d human mesh regression with dense correspondence. In *Proceedings of the IEEE/CVF conference on computer vision and pattern recognition*, pages 7054–7063, 2020. 6
- [59] Hongwen Zhang, Yating Tian, Xinchu Zhou, Wanli Ouyang, Yebin Liu, Limin Wang, and Zhenan Sun. Pymaf: 3d human pose and shape regression with pyramidal mesh alignment feedback loop. In *Proceedings of the IEEE/CVF International Conference on Computer Vision*, pages 11446–11456, 2021. 1, 2, 6
- [60] Hongwen Zhang, Yating Tian, Yuxiang Zhang, Mengcheng Li, Liang An, Zhenan Sun, and Yebin Liu. Pymaf-x: Towards well-aligned full-body model regression from monocular images. *IEEE Transactions on Pattern Analysis and Machine Intelligence*, 2023. 1, 6
- [61] Jinlu Zhang, Zhigang Tu, Jianyu Yang, Yujin Chen, and Junsong Yuan. Mixste: Seq2seq mixed spatio-temporal encoder for 3d human pose estimation in video. In *Proceedings of the IEEE/CVF conference on computer vision and pattern recognition*, pages 13232–13242, 2022. 5
- [62] Zhenyu Zhang, Wenhao Chai, Zhongyu Jiang, Tian Ye, Mingli Song, Jenq-Neng Hwang, and Gaoang Wang. Mpm: A unified 2d-3d human pose representation via masked pose modeling. *arXiv preprint arXiv:2306.17201*, 2023. 2, 5
- [63] Long Zhao, Xi Peng, Yu Tian, Mubbasir Kapadia, and Dimitris N Metaxas. Semantic graph convolutional networks for 3d human pose regression. In *Proceedings of the IEEE/CVF conference on computer vision and pattern recognition*, pages 3425–3435, 2019. 1, 2, 5
- [64] Zhonghan Zhao, Wenhao Chai, Shengyu Hao, Wenhao Hu, Guanhong Wang, Shidong Cao, Mingli Song, Jenq-Neng Hwang, and Gaoang Wang. A survey of deep learning in sports applications: Perception, comprehension, and decision. *arXiv preprint arXiv:2307.03353*, 2023. 1
- [65] Ce Zheng, Sijie Zhu, Matias Mendieta, Taojiannan Yang, Chen Chen, and Zhengming Ding. 3d human pose estimation with spatial and temporal transformers. In *Proceedings of the IEEE/CVF International Conference on Computer Vision*, pages 11656–11665, 2021. 1
- [66] Zhuoran Zhou, Zhongyu Jiang, Wenhao Chai, Cheng-Yen Yang, Lei Li, and Jenq-Neng Hwang. Efficient domain adaptation via generative prior for 3d infant pose estimation, 2023. 2

UniHPE: Towards Unified Human Pose Estimation via Contrastive Learning

Supplementary Material

A. Details of Singular Value based Loss

In this paper, we propose a singular value based contrastive learning loss to align more than two modalities simultaneously. In this section, more details of the singular value based loss are discussed, including training speed and hyperparameters.

Training Speed. We compare the training speed difference per batch on the Nvidia A100 with three different loss setup: \mathcal{L}_{pair} only, $\mathcal{L}_{pair} + \mathcal{L}_{triplet}$ with singular values, and $\mathcal{L}_{pair} + \mathcal{L}_{triplet}$ with eigenvalues. As shown in Table 7, the eigenvalue based $\mathcal{L}_{triplet}$ does not significantly increase

Loss	Per Batch Time (s)
\mathcal{L}_{pair}	1.77
$\mathcal{L}_{pair} + \mathcal{L}_{triplet}$ (singular value)	2.64 (+49.1%)
$\mathcal{L}_{pair} + \mathcal{L}_{triplet}$ (eigenvalue)	2.01 (+13.5%)

Table 7. Per batch training speed with Nvidia A100. The proposed $\mathcal{L}_{triplet}$ does not significantly increase the training complexity and can be easily adopted to other multi-modal alignment training pipelines

the training complexity and can be easily adopted to other multi-modal alignment training pipelines.

Hyperparameters. In each batch B , for every triplet of data, we randomly sample $B - 1$ negative triplets. Therefore, eigenvalues of $B \times B$ matrices are calculated. In our experiment, the weight, α , of $\mathcal{L}_{triplet}$ is 1 and the learnable temperature, τ , is shared with \mathcal{L}_{pair} .

B. Architecture Details

In this section, we introduce the detailed architectures of 2D and 3D pose encoders and decoders.

The bounding box token. According to [28], without bounding box information, different 3D human poses may have exact the same 2D human poses in the cropped bounding box. Therefore, in our 2D encoder and 2D decoder, there is an additional bounding box token to provide bounding box information.

B.1. MLP Encoders and Decoders

We implement MLP with residual blocks as our MLP encoders and decoders, as shown in Fig 9. The MLP en-

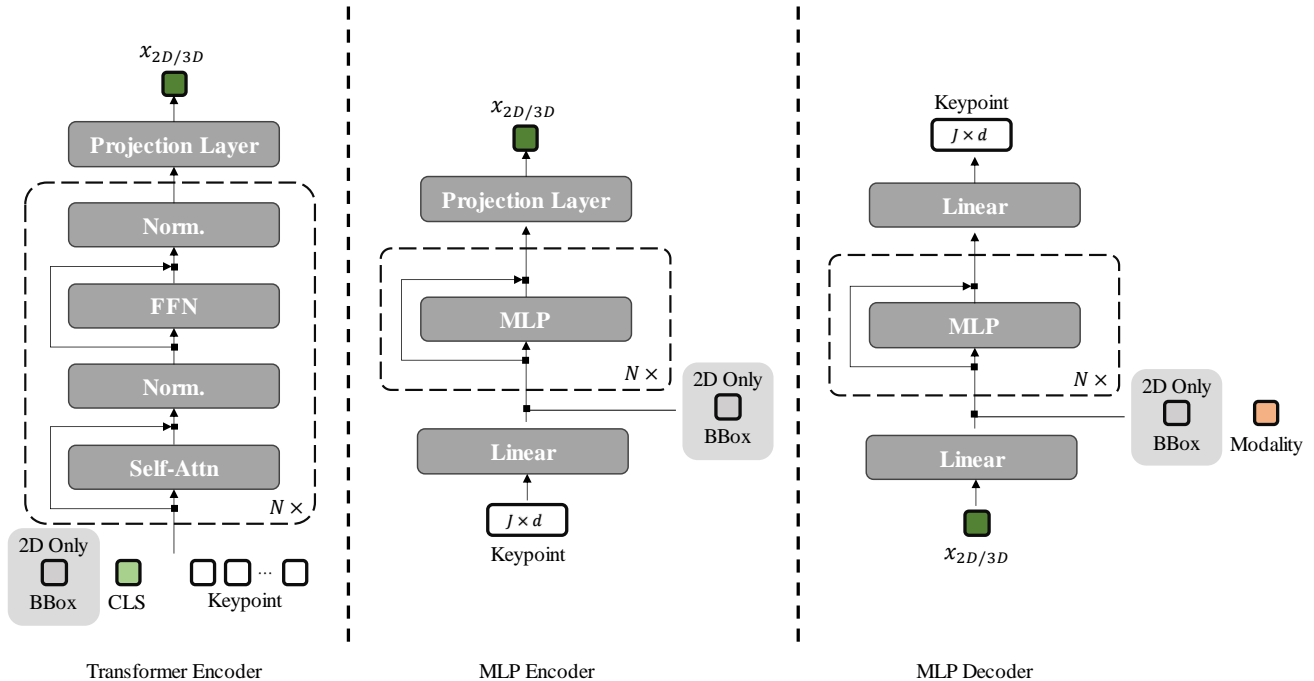


Figure 8. The architectures of the transformer based encoder and MLP based encoder and decoder.

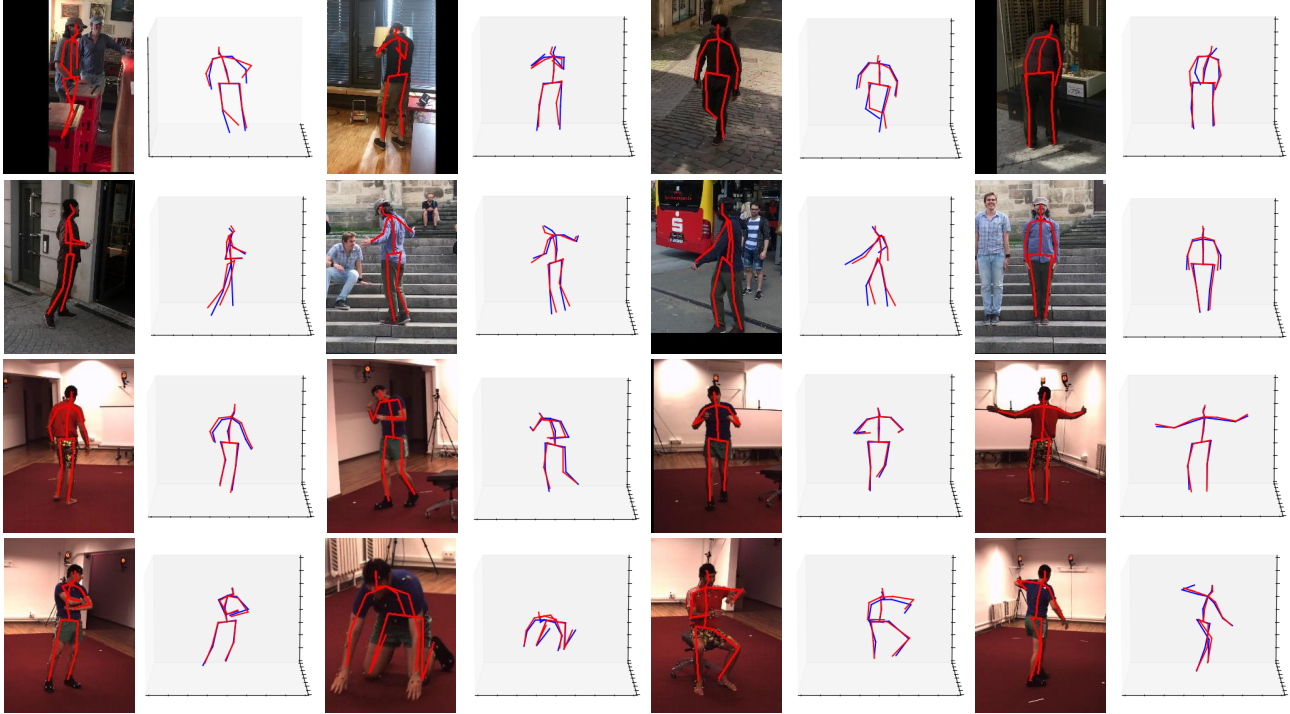


Figure 9. More visualization of our method. The first two rows are from 3DPW dataset, while the last two rows are from Human3.6M dataset. The red skeleton is the ground truth, and the blue one is estimated from the image branch.

coder and decoder are constructed with 3 MLP with residual blocks. As mentioned in Sec 3, there is a modality token, \mathcal{M} , which indicates the input modality to further boost the performance.

B.2. Transformer Encoders

For pose encoding, our 2D and 3D transformer encoders share similar architectures, except the 2D encoder takes an additional bounding box token as input to solve the projection ambiguity. A $[CLS]$ token, J keypoint tokens projected from 2D and 3D keypoints, and an additional bounding box token for the 2D encoder are the input of the encoder. After three transformer encoder layers with multi-head attention, the embedding of the $[CLS]$ token is projected to the shared feature space with dimension as 1024.

B.3. Diffusion Decoders

We apply the same architecture as GFpose[5] and Score Matching Network [45] as our diffusion decoders with an additional bounding box token and modality token. The decoder supposedly recovers accurate keypoints from random Gaussian noise by giving the previous resulting tokens as conditions. We set the timestep, t , in $(0, 1]$ and uniformly sample the timestep 1000 times in training and inference. Different from the original GFpose, our keypoints are de-

finned as pelvis-relative in the camera coordinate.